Electronic Supplementary Material (ESI) for Physical Chemistry Chemical Physics.

Supporting Information for "Influence of surface nanostructure-induced innermost ion structuring on capacitance of carbon/ionic liquid double layers"

Yi-Jung Tu* and Shen-Ting Peng

Department of Applied Chemistry, National Chi Nan University, Puli, Nantou, Taiwan 54561

E-mail: yjtu@ncnu.edu.tw

1 NPT density equilibration

We performed Monte Carlo simulations to equilibrate the the ionic liquid (IL) density enclosed between two "frozen" carbon electrodes with perfectly flat graphene or nanostructured surface. Simulations were performed with neat [$BMIm^+$][$TFSI^-$] and [$BMIm^+$][FSI^-] ILs. The lengths of these simulation cells obtained from NPT density equilibration are summarized in Table S1 for [$BMIm^+$][$TFSI^-$] and Table S2 for [$BMIm^+$][FSI^-].

Table S1: The system sizes and cell lengths for neat [$BMIm^+$][$TFSI^-$]

electrode surface	number of ion pairs	L_{cell} (nm)	L_{gap}[c](nm)
flat graphene[1]	400	9.84[a]	14.20
S1	400	10.74[b]	13.30
S2[2]	400	10.83[b]	9.21

[a] the distance between two graphene sheets after MC equilibration.
[b] the distance between the graphene sheets of the two nanostructured electrodes after MC equilibration.
[c] the distance across the vacuum region after MC equilibration.

Table S2: The system sizes and cell lengths for neat [$BMIm^+$][FSI^-]

electrode surface	number of ion pairs	L_{cell} (nm)	L_{gap}[c](nm)
flat graphene	400	7.99[a]	16.05
S2	400	9.01[b]	15.04

[a] the distance between two graphene sheets after MC equilibration.
[b] the distance between the graphene sheets of the two nanostructured electrodes after MC equilibration.
[c] the distance across the vacuum region after MC equilibration.

2 Fixed-voltage approach

We present details of our fixed-voltage MD approach[3] described in the manuscript. Our simulation cell setup is to use 3D periodic boundary conditions for electrostatics. Along the z dimension, the simulation cell is divided into two regions: the first region is the electrochemical cell of interest, and the second region is a vacuum gap that separates the

periodic replica of the electrochemical cell. These two regions are denoted as "cell" and "gap". The advantage of this setup is that the change in electrostatic potential is zero over a periodic translation. As we set the voltage drop across the cell to the external potential $\Delta V_{cell} = \Delta V_{applied}$, the voltage drop over the vacuum is $-\Delta V_{applied}$. The electrochemical cell will be held at a specified voltage drop if the electric field in the vacuum region is $E_z^{gap} = -\Delta V_{applied}/L_{gap}$, where $\Delta V_{applied}$ is the desired voltage drop over the cell, and L_{gap} is the distance across the vacuum gap.

Because the carbon atom chains of the electrodes are not conducting, the voltage drop across the cell (ΔV_{cell}) is fixed between the two conducting graphene electrode sheets. For modeling the graphene electrodes at fixed voltage, the boundary condition is enforced at the discrete points of the conducting sheets on either side of the vacuum gap by solving for the surface charges. A unique solution is guaranteed[4] such that $E_z^{gap} = -\Delta V_{applied}/L_{gap}$, which therefore enforces $\Delta V_{cell} = \Delta V_{applied}$.

In practice, we assign a Gaussian pillbox to each carbon atom on the conducting graphene electrodes. We assume that the normal component of the electric field (E_z) is uniform over the pillbox surface and produces a field of $\sigma_i/2\epsilon_0$. The charge density corresponding to the pillbox surface is $\sigma_i = q_i/a$, where q_i is the charge on the ith graphene atom, and $a = A/N_{atom}$ is the effective surface area per graphene atom given by the area of the sheet (A) divided by the number of atoms per sheet (N_{atom}). To enforce the boundary condition at graphene electrodes, we write the total electric field at the pillbox surface as a contribution from the surface charge on the ith graphene atom, $\sigma_i/2\epsilon_0$, and from all other charges, $E_z^{i,external}(\mathbf{r}_{Ni}, \{\sigma_j\})$. The external field, $E_z^{i,external}(\mathbf{r}_{Ni}, \{\sigma_j\})$, is computed from a 3D-PME sum and is a function of the positions of all electrolyte atoms ($\mathbf{r}_{Ni}$) as well as the set of surface charges of the conducting electrodes ($\{\sigma_j\}$). We set the total field equal to $E_z^{gap} = -\Delta V_{applied}/L_{gap}$ and rearrange to get the charge on each graphene atom

$$q_i = \pm 2a\epsilon_0\left(\frac{\Delta V_{applied}}{L_{gap}} + E_z^{i,external}(\mathbf{r}_{Ni}, \{\sigma_j\})\right) \tag{S1}$$

The plus/minus sign in eq S1 corresponds to charges on the positive/negative electrode, respectively. Equation S1 must be iteratively solved, with a 3D-PME sum recomputed at each iteration to update $E_z^{i,external}(\mathbf{r}_{Ni}, \{\sigma_j\})$. As discussed in a previous work,[3] the conducting graphene sheets are kept perfectly flat so that the electric field across each pillbox surface is entirely from the z-component.

3 Charge density and Poisson potential profiles

We follow our previously developed protocols to compute the differential capacitance of each electrical double layer (EDL).[1] To do this, we determine the total charge on each electrode and the voltage drop across the EDL at the electrode. At each voltage applied between electrodes of an electrochemical cell (ΔV_{cell}), the total surface charges on the two electrodes can be directly obtained from the outputs of fixed-voltage MD simulations. To determine the EDL voltage drop at each electrode, we calculate the 1-D Poisson potential profile between the two electrodes of the electrochemical cell. In Figure S1, we show a Poisson potential profile for neat [$BMIm^+$][$TFSI^-$] at applied voltage between electrodes (ΔV_{cell}) of 4 V, and the definition of EDL voltage drops for the two electrodes. Since the potential is constant in the bulk region of the profile, the EDL voltage drop at the positive and negative electrodes can be clearly determined from the potential difference between the electrode and the bulk IL, which are denoted as $\Delta V_{positive}$ and $\Delta V_{negative}$, respectively. Note that all ΔV_{cell} values are corrected with the potential of zero charge (PZC), the potential difference between the electrode and the bulk IL region for simulations at 0 volt. This correction does not affect the differential capacitance as the effect of PZCs is subtracted out by calculating the deviation of any two voltage drops, but we use the PZC-corrected $\Delta V_{positive}$ and $\Delta V_{negative}$ values to report the electrode potential throughout this work.

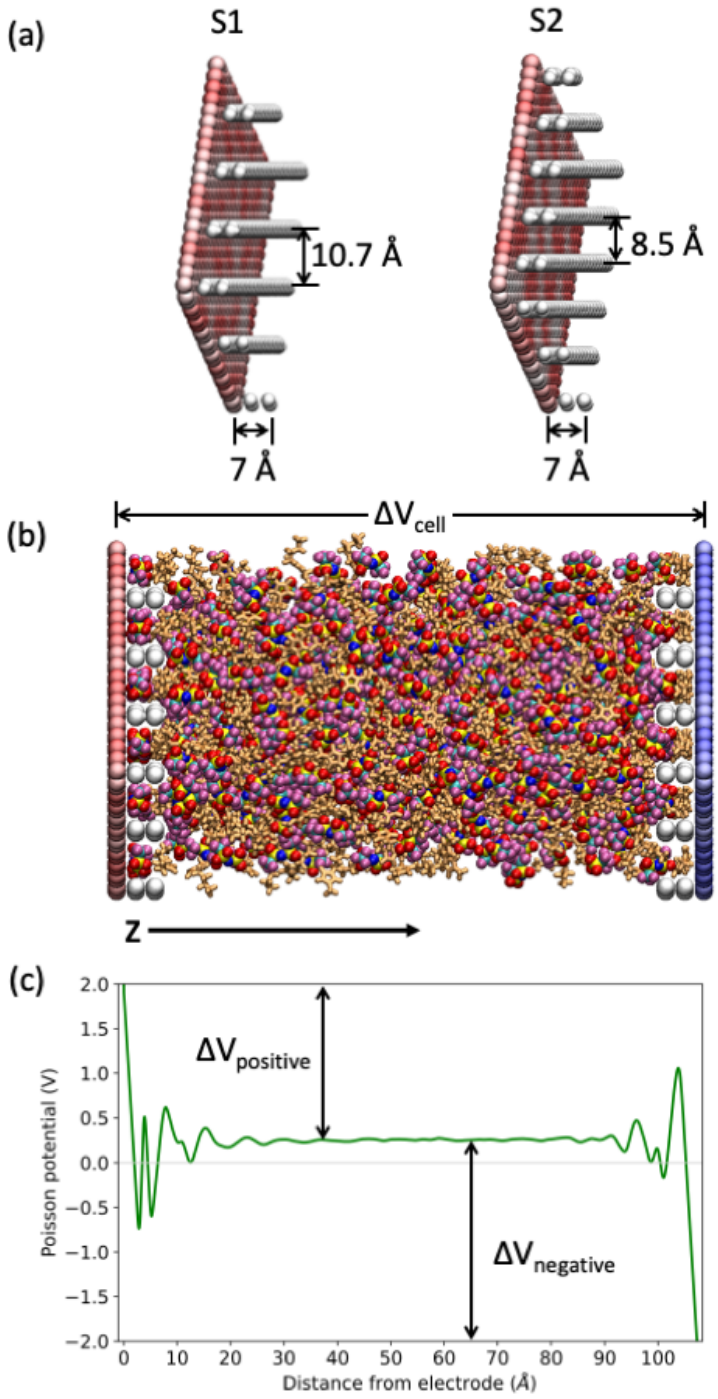

Figure S1: (a) Roughness scales of the S1 and S2 carbon electrode surfaces; (b) a snapshot of MD simulation for the S1/[$BMIm^+$][$TFSI^-$] electrochemical system and (c) the Poisson potential across the two electrodes with $\Delta V_{cell} = 4$ Volt.

To investigate the voltage-dependent capacitance for ionic liquid double layers, fixed voltage MD simulations were performed at different voltages ranging from 0 to ∼4.5 V applied

across the electrochemical cell. Figures S2 shows the profiles for charge density distribution and its Poisson potential of the S1/[$BMIm^+$][$TFSI^-$] interface at different applied voltages. For [$BMIm^+$][FSI^-], the profiles of the flat graphene and S2 electrodes are shown in Figures S3 and S4, respectively. Here, we only present the charge density distribution and Poisson potential profiles for each electrochemical system at 0/0, –1/1, and –2/2 V. The decomposed $\Delta V_{positive}$ and $\Delta V_{negative}$ at all investigated applied voltages are summarized in Table S3 for the S1/[$BMIm^+$][$TFSI^-$] interface, Table S4 for the graphene/[$BMIm^+$][FSI^-] interface, and Table S5 for the S2/[$BMIm^+$][FSI^-] interface.

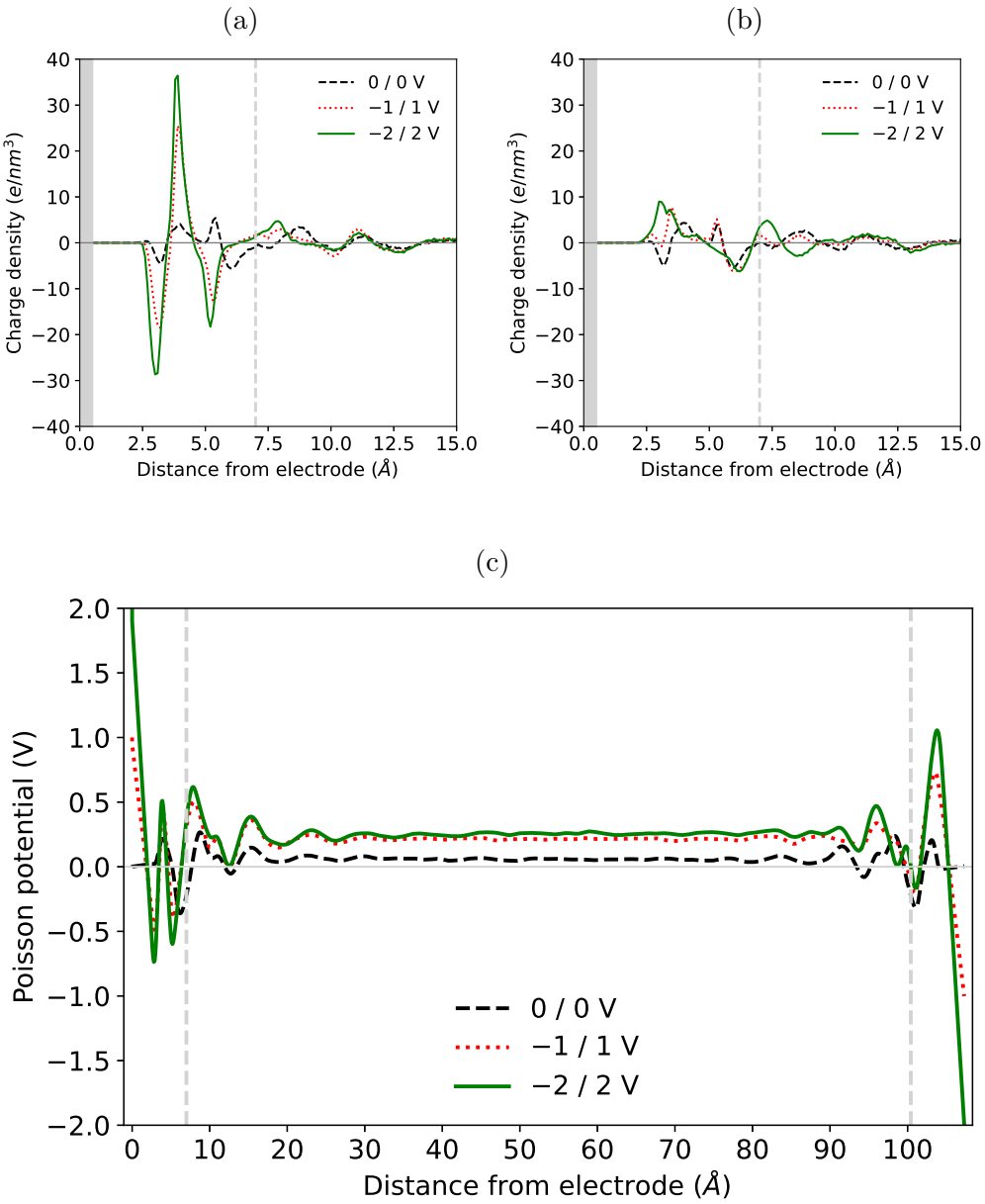

Figure S2: The charge distribution profiles of neat [$BMIm^+$][$TFSI^-$] (a) near the positive and (b) negative electrodes as a function of applied voltage between electrodes from 0/0 to –2/2 V. (c) The potential profiles computed for the charge density distributions shown in (a) and (b). The vertical dashed lines indicate the depth of nanochannels of the S1 electrode.

Table S3: The electrode surface charge and EDL voltage drops as a function of applied voltage between electrodes for the S1/[BMIm$^+$][TFSI$^-$] system

ΔV_{cell}	Q	$\Delta V_{negative}$	$\Delta V_{positive}$
0/0 V	–0.11 e	–0.06 V	–0.06 V
–0.25/0.25 V	1.33 e	–0.35 V	0.15 V
–0.75/0.75 V	4.58 e	–0.89 V	0.61 V
–1/1 V	6.14 e	–1.21 V	0.79 V
–1.25/1.25 V	7.54 e	–1.46 V	1.04 V
–1.5/1.5 V	8.76 e	–1.76 V	1.24 V
–1.75/1.75 V	10.27 e	–1.93 V	1.57 V
–2/2 V	11.66 e	–2.25 V	1.75 V

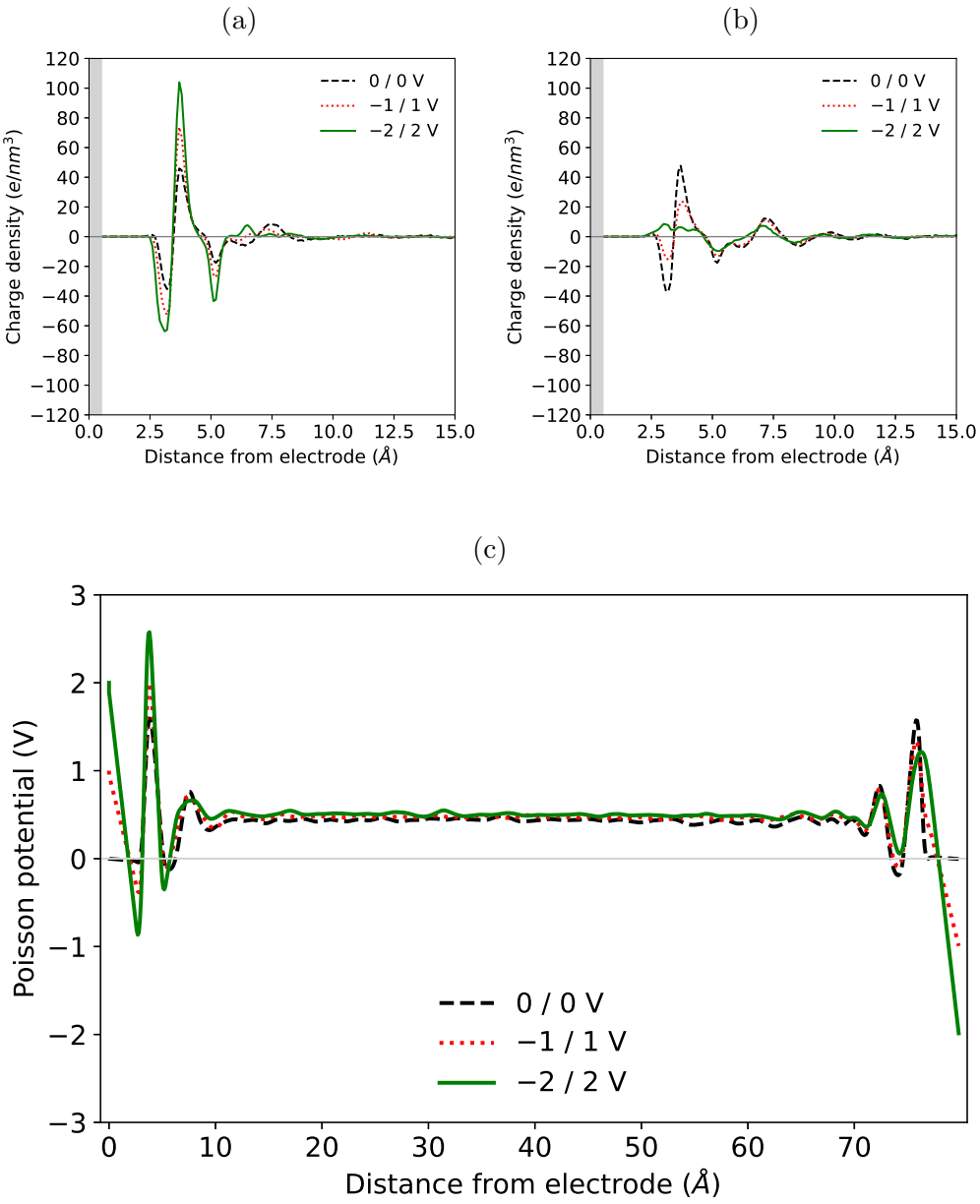

Figure S3: The charge distribution profiles of neat [$BMIm^+$][FSI^-] (a) near the positive and (b) negative electrodes as a function of applied voltage between the graphene electrodes from 0/0 to –2/2 V. (c) The potential profiles computed for the charge density distributions shown in (a) and (b).

Table S4: The electrode surface charge and EDL voltage drops as a function of applied voltage between electrodes for the graphene/[$BMIm^+$][FSI^-] system

ΔV_{cell}	Q	$\Delta V_{negative}$	$\Delta V_{positive}$
0/0 V	0.10 e	–0.43 V	–0.43 V
–0.25/0.25 V	1.14 e	–0.65 V	–0.15 V
–0.75/0.75 V	4.17 e	–1.16 V	0.34 V
–1/1 V	5.86 e	–1.47 V	0.53 V
–1.75/1.75 V	10.60 e	–2.21 V	1.29 V
–2/2 V	12.45 e	–2.50 V	1.50 V

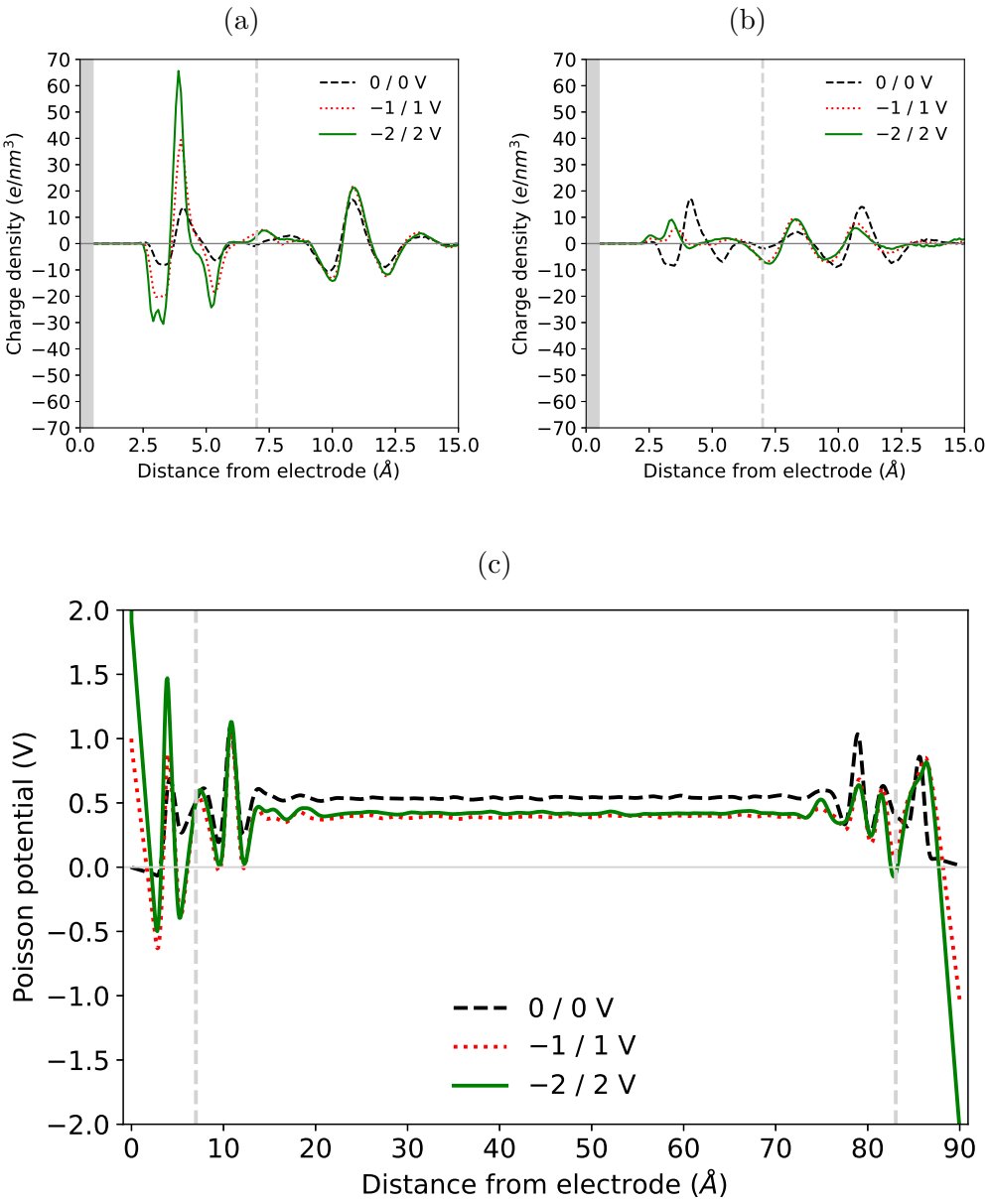

Figure S4: The charge distribution profiles of neat [$BMIm^+$][FSI^-] (a) near the positive and (b) negative electrodes as a function of applied voltage between electrodes from 0/0 to –2/2 V. (c) The potential profiles computed for the charge density distributions shown in (a) and (b). The vertical dashed lines indicate the depth of nanochannels of the S2 electrode.

Table S5: The electrode surface charge and EDL voltage drops as a function of applied voltage between electrodes for the S2/[$BMIm^+$][FSI^-] system

ΔV_{cell}	Q	$\Delta V_{negative}$	$\Delta V_{positive}$
0/0 V	0.24 e	–0.54 V	–0.54 V
–0.25/0.25 V	1.71 e	–0.81 V	0.31 V
–0.75/0.75 V	5.09 e	–1.21 V	0.29 V
–1/1 V	6.84 e	–1.39 V	0.61 V
–1.5/1.5 V	9.14 e	–1.96 V	1.04 V
–1.75/1.75 V	10.18 e	–2.23 V	1.27 V
–2/2 V	10.78 e	–2.42 V	1.58 V
–2.25/2.25 V	11.60 e	–2.75 V	1.75 V

In Figure S5 and Figure S6, we show comparison of the capacitance profiles of the flat graphene and nanostructured carbon electrodes for [$BMIm^+$][$TFSI^-$] and [$BMIm^+$][FSI^-], respectively. Note that the capacitance values in Figures S5 and S6 are normalized by the surface area (2103 $Å^2$) of the graphene sheet, although the carbon chains on the nanostructured electrode surfaces are not conducting and the space between the carbon chains and the graphene sheets is inaccessible to the IL molecular ions.

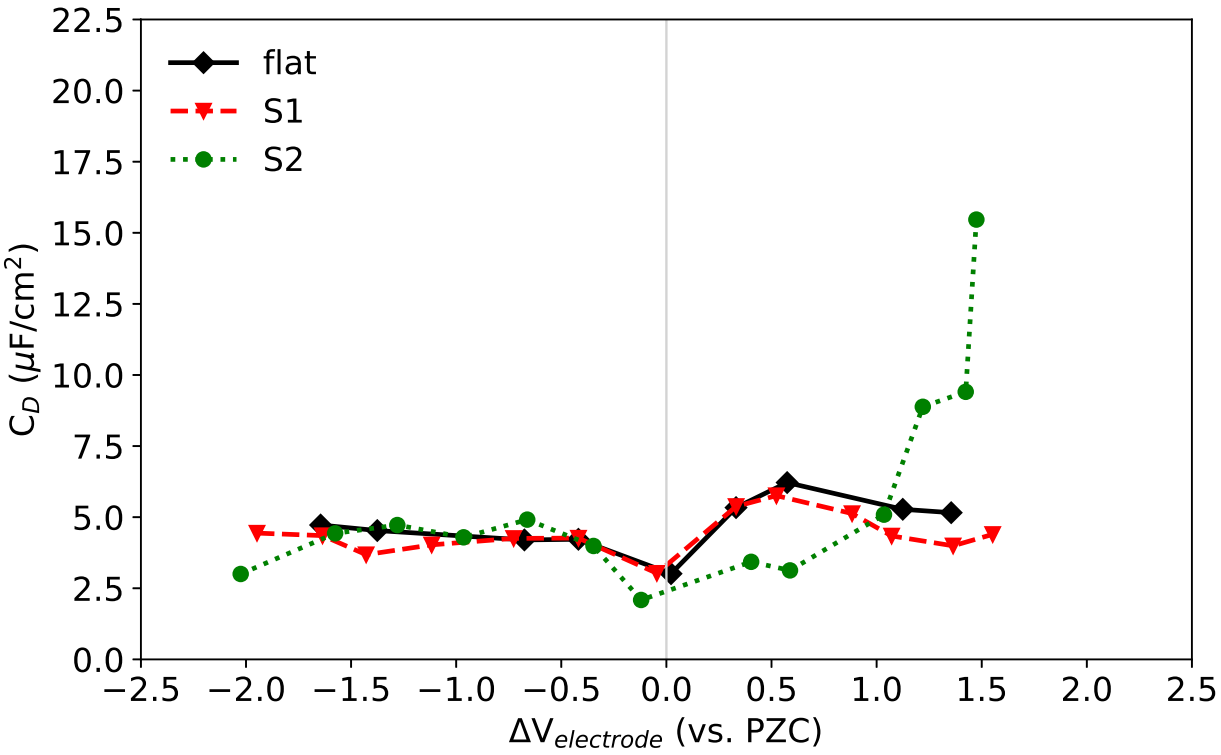

Figure S5: Differential capacitance of pure [BMIm$^+$][TFSI$^-$] at flat graphene[1] (black curve), S1 (red curve), and S2[2] (green curve) electrodes plotted as a function of electrode potential, relative to the PZC.

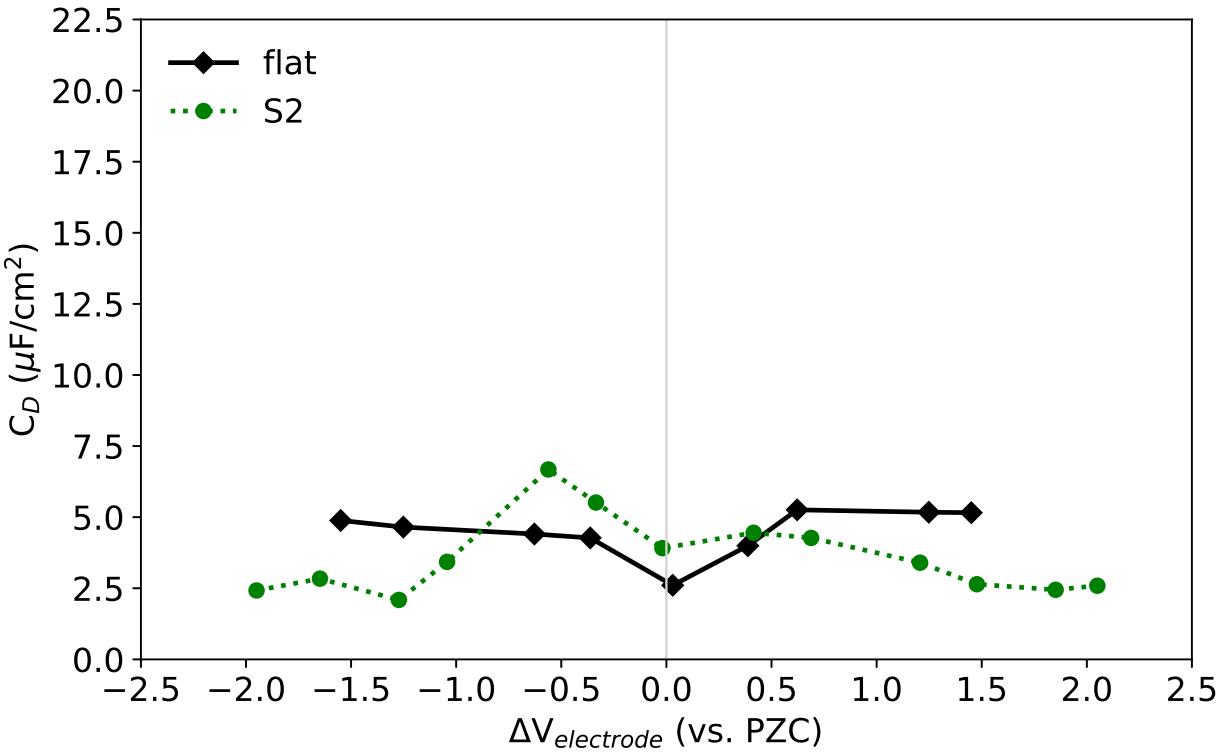

Figure S6: Differential capacitance of pure [$BMIm^+$][FSI^-] at flat graphene (black curve) and S2 (green curve) electrodes plotted as a function of electrode potential, relative to the PZC.

4 Radial distribution functions (RDFs)

We compute RDFs of interfacial ions to characterize the interactions of different ions near the electrode surface. The RDF is defined as

$$g_{\alpha\beta}(r) = \frac{1}{N_\alpha \rho_\beta} \sum_{i=1}^{N_\alpha} \sum_{j=1}^{N_\beta} \frac{1}{4\pi r^2} \langle \delta(r_{ij} - r) \rangle \tag{S2}$$

where α and β denote atom types, N_α is the number of atoms for type α, and ρ_β=N_β/V is the density of atoms of type β. For RDFs computed for anions/cations around adsorbed ions, N_α is the number of atoms for the ions that are located within surface channels, and N_β is the number of atoms for particular type of the cations or anions.

It is important to note that the volume "V" used for the normalization of the RDFs is somewhat ill-defined. As the main purpose of RDFs is to indicate and compare different types of ionic correlations at a given electrode interface, we normalize the RDFs by simply using the volume of the entire simulation cell, which includes the vacuum gap, carbon chains, and inaccessible surface area of graphene sheets.

4.1 Anion-Anion RDF for Interfacial FSI^- Anions

Figure S7 shows the RDFs computed for FSI^- anions at the S2 electrode interface.

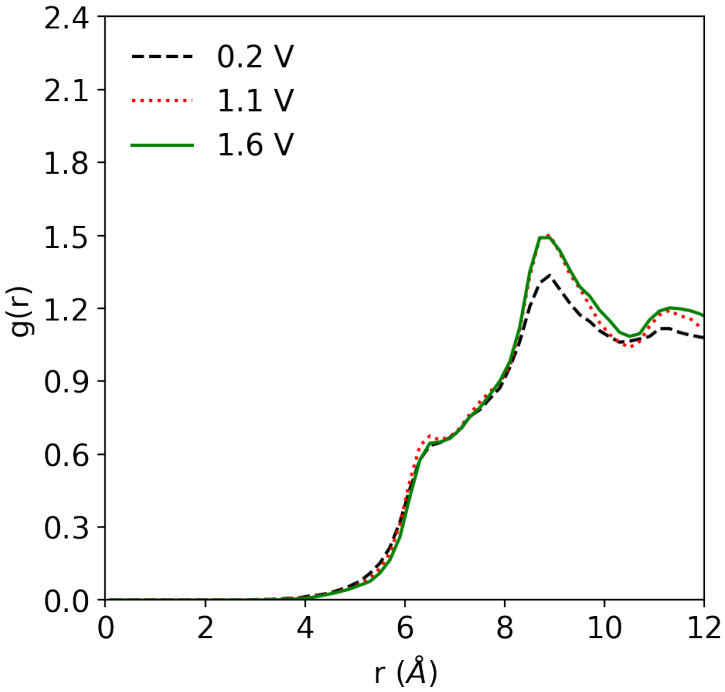

Figure S7: Anion-anion radial distribution functions (RDFs) computed from fluorine atoms of interfacial FSI^- anions near the positive electrode as a function of applied voltage. The anion/anion RDF are computed for FSI^- anions whose center of mass are within 7 Å of the graphene surface.

5 Density Profiles of IL Functional Groups

In Figure S8, we present the density distribution plots for the functional groups of $BMIm^+$ cations and $TFSI^-$ anions near the S1 electrode surface at positive polarization. The mag-

nitude and location of each density peak indicate the type of interaction of ions with the electrode at each applied voltage. At low voltage, the nonpolar $–C_4H_9$ groups of $BMIm^+$ and the nonpolar $–CF_3$ groups of $TFSI^–$ are in contact with the graphene surface of the S1 electrode. At higher positive potential, $TFSI^–$ anions keep the $–CF_3$ groups in contact with graphene when their charged $–SO_2$ groups orient toward the positive surface. This voltage-mediated structural rearrangement of $TFSI^–$ anions blocks the nonpolar $–C_4H_9$ groups of $BMIm^+$ from the graphene surface of the S1 electrode, but moves the imidazolium rings closer to the positive electrode because of electrostatic interaction of the adsorbed $TFSI^–$ anions with $BMIm^+$ cations.

Figure S9 shows the structural rearrangement of $[BMIm^+][TFSI^–]$ at the S1 electrode interface, but for negative polarization. With increasing negative polarization, there is a clear shift in the functional group distribution of $BMIm^+$cations, as the imidazolium rings are pulled into close contact with the negative electrode surface. At large negative potential, the $TFSI^–$ anions are completely removed from the electrode surface, but they are not fully separated from the $BMIm^+$ cations located within the channels; the charged/polar $–SO_2$ groups of $TFSI^–$ anions coordinate with the imidazolium rings of the adsorbed $BMIm^+$ cations at the negative electrode. Such cation/anion interactions lead to charge cancellation of cations and anions in the $[BMIm^+][TFSI^–]$ double layers, as shown by the charge density analysis in Figure S2b.

We present similar functional group distribution analysis for $[BMIm^+][FSI^–]$ at the S2 electrode interface. The density distribution profiles for $FSI^–$ and $BMIm^+$ functional groups near the S2 electrode are shown in Figures S10 and S11 for positive and negative polarizations. respectively.

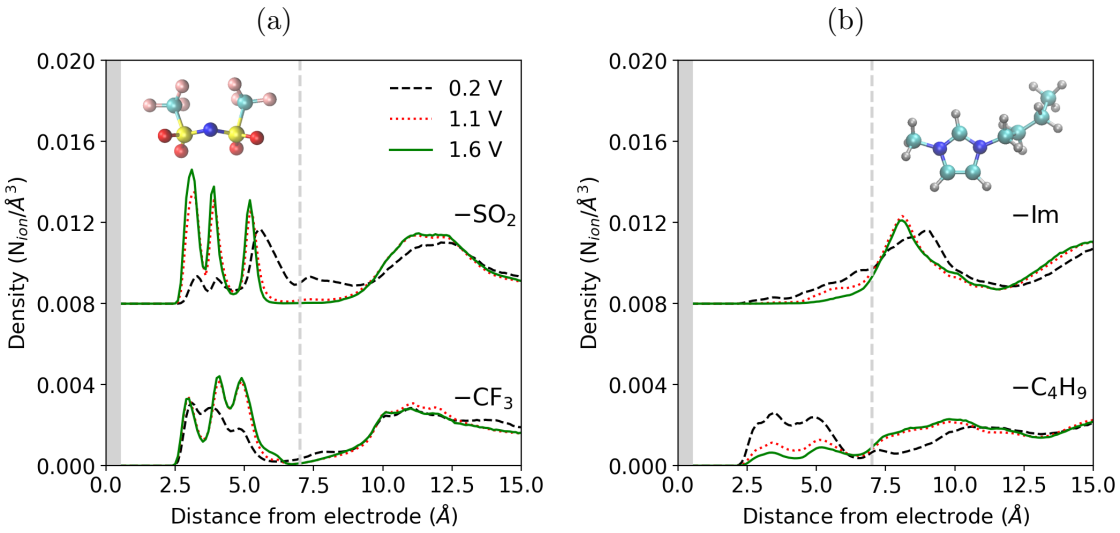

Figure S8: Functional group distribution profiles of interfacial (a) $TFSI^-$ anions and (b) $BMIm^+$ cations near the S1 electrode as a function of positive electrode potential. The density plots for –SO_2 and –Im are shifted by 0.008 for clarity.

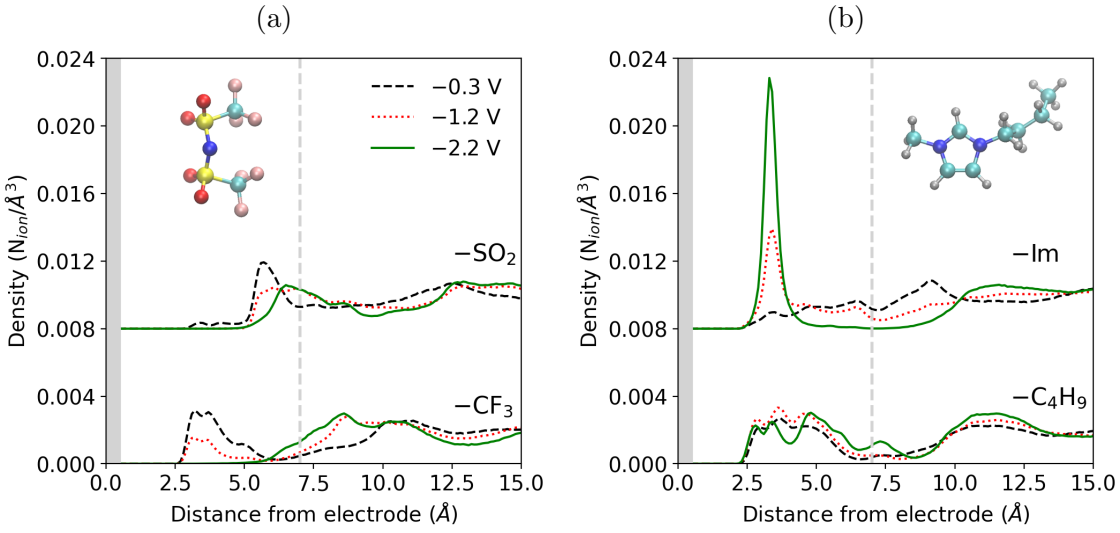

Figure S9: Functional group distribution profiles of interfacial (a) $TFSI^-$ anions and (b) $BMIm^+$ cations near the S1 electrode as a function of negative electrode potential. The density plots for –SO_2 and –Im are shifted by 0.008 for clarity.

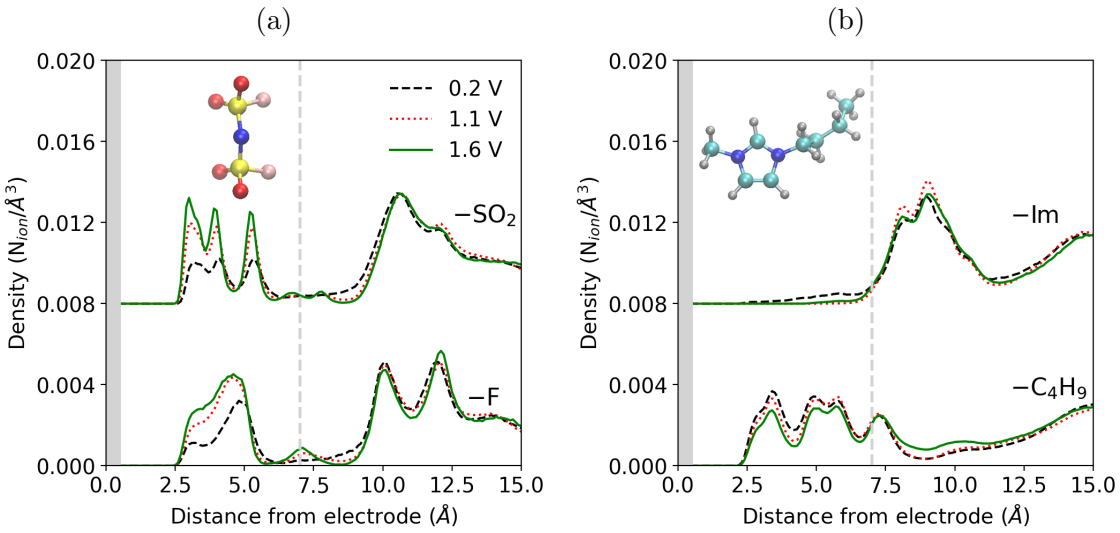

Figure S10: Functional group distribution profiles of interfacial (a) FSI^- anions and (b) $BMIm^+$ cations near the S2 electrode as a function of positive electrode potential. The density plots for –SO_2 and –Im are shifted by 0.008 for clarity.

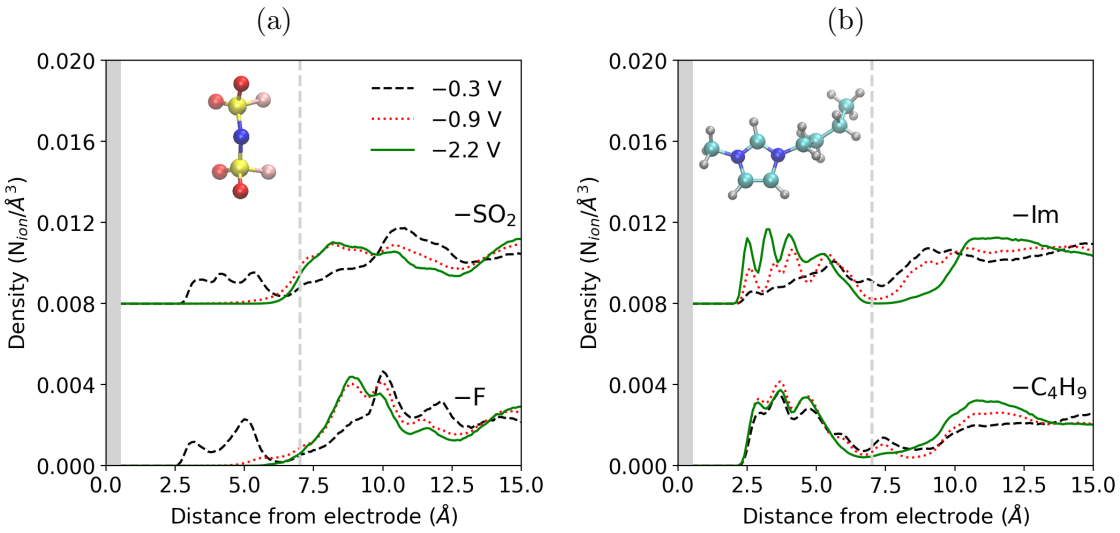

Figure S11: Functional group distribution profiles of interfacial (a) FSI^- anions and (b) $BMIm^+$ cations near the S2 electrode as a function of negative electrode potential. The density plots for –SO_2 and –Im are shifted by 0.008 for clarity.

References

(1) Tu, Y.-J.; McDaniel, J. G. Structure–Capacitance Relationships of Graphene/Ionic Liquid Electrolyte Double Layers. *J. Phys. Chem. C* **2021**, *125*, 20204–20218.

(2) Tu, Y.-J.; Wu, S.-C.; McDaniel, J. G. Importance of Anion–Anion Pairing for Capacitance of Carbon/Ionic Liquid Interfaces. *J. Phys. Chem. C* **2022**, *126*, 20213–20225.

(3) Tu, Y.-J.; Delmerico, S.; McDaniel, J. G. Inner Layer Capacitance of Organic Electrolytes from Constant Voltage Molecular Dynamics. *J. Phys. Chem. C* **2020**, *124*, 2907–2922.

(4) Jackson, J. D. *Classical Electrodynamics*, 3rd ed.; Wiley: New York, NY, 1999.